Injectable Hydrogel Scaffold Incorporating Microspheres Containing Cobalt-Doped Bioactive Glass for Bone Healing

Parmida Ghiasi Tabari[1]

Amirmohammad Sattari[2]

Mohsen Mashhadi Keshtiban[3]

Nushin Karkuki Osguei[4]

John G. Hardy[5,6]

Ali Samadikuchaksaraei[1*]

1. Department of Medical Biotechnology, Faculty of Allied Medicine, Iran University of Medical Sciences, Tehran, Iran

2. Department of Mechanical Engineering, K. N. Toosi University of Technology, Tehran, Iran

3. School of Mechanical Engineering, College of Engineering, University of Tehran, Iran

4. Eposcience Millennium Institute, Tehran, Iran

5. Department of Chemistry, Lancaster University, Lancaster, UK

6. Materials Science Lancaster, Lancaster University, Lancaster, UK

***Corresponding author:**

Ali Samadikuchaksaraei (ORCID: 0000-0002-2108-9927)

Department of Medical Biotechnology, Faculty of Allied Medicine, Iran University of Medical Sciences, Tehran 1449614535, Iran

Tel: (+98 21) 8670 4556

E-mails: samadikuchaksaraei@yahoo.com; ali.samadi@iums.ac.ir

Running title:

Hydrogel for Bone Regeneration

Abstract

Injectable in-situ-forming scaffolds that induce both angiogenesis and osteogenesis have been proven to be promising for bone healing applications. Here, we report the synthesis of an injectable hydrogel containing cobalt-doped bioactive glass-loaded microspheres. Silk fibroin/gelatin microspheres containing bioactive glass particles (BGs) were fabricated through microfluidics. The microspheres were mixed in an injectable alginate solution, which formed an in-situ hydrogel by adding $CaCl_2$. The hydrogel was evaluated for its physicochemical properties, in vitro interactions with osteoblast-like and endothelial cells, and bone healing potential in a rat model of calvarial defect. The microspheres were well-dispersed in the hydrogel and formed pores of > 100 μm. The hydrogel displayed shear-thinning behavior and modulated the cobalt release so that the optimal cobalt concentration for angiogenic stimulation, cell proliferation and deposition of mineralized matrix was only achieved by the scaffold that contained BG doped with 5% w/w cobalt (A-S-G5Co). In the scaffold containing higher cobalt content, a reduced biomimetic mineralization on the surface was observed. The gene expression study indicated an upregulation of the osteogenic genes of COL1A1, ALPL, OCN and RUNX2 and angiogenic genes of HIF1A and VEGF at different time points in the cells cultured with the A-S-G5Co. Finally, the in vivo study demonstrated that A-S-G5Co significantly promoted both angiogenesis and osteogenesis and improved bone healing after 12 weeks of follow-up. These results show that incorporation of silk fibroin/gelatin microspheres containing cobalt-doped BG in an injectable in-situ-forming scaffold can effectively enhance its bone healing potential through promotion of angiogenesis and osteogenesis.

Keywords: Hydrogels; Microspheres; Cobalt; Osteogenesis; Angiogenesis

Introduction

Applications of bone tissue engineering scaffolds have been established in several clinical and experimental settings. The scaffold should promote not only osteogenesis, but also angiogenesis in order to improve bone healing[1]. If the scaffold is designed to be injectable and in situ-forming, it offers several advantages, including filling defects of any shape, adhering to the surrounding tissue, and minimizing the need for aggressive surgical procedures[2,3]. However, injectable scaffolds cannot provide adequate mechanical support if they are not specifically designed for this purpose.

One of the methods to enhance the mechanical properties and fine-tune the pore size of injectable scaffolds involves utilizing the structural interactions and connections formed by microspheres[4]. Also, incorporation of microspheres into bone scaffolds enables a bottom-up fabrication approach. Microspheres could be synthesized by water-in-oil microfluidic emulsification, which allows precise control over their size, shape, and composition, leading to formation of uniform and well-defined structures[5]. Additionally, uniform distribution of microspheres, loaded with bioactive molecules and ions, throughout the scaffold, facilitates enhanced control over their release[4].

For synthesis of microspheres, the materials used for the aqueous phase of water-in-oil emulsification, should be able to form a stable emulsion with the oil phase and be polymerizable or crosslinkable to form solid microspheres. Silk fibroin (SF) and gelatin (G) have been shown to possess these properties[6] and to support bone healing[7,8]. Microspheres synthesized from SF/G could be reinforced for their osteoinductive and osteoconductive properties by loading with various materials such as bioactive glass (BG) particles[1].

When developing a regenerative strategy to promote bone repair, the significance of angiogenesis should be considered. It has been shown that a functional interplay, defined as

angiogenesis-osteogenesis coupling, plays a key role in the healing bone[9,10]. One strategy for induction of angiogenesis is to dope BG particles with angiogenic ions such as cobalt[11]. This enhances angiogenesis by mimicking a hypoxic state and activating hypoxia-inducible factor 1α (HIF-1α)[12]. Despite various strategies in bone tissue engineering, combining angiogenesis and osteogenesis in a single injectable scaffold remains a challenge. Here, we propose a novel approach by fabricating a microsphere-containing injectable in situ-forming hydrogel scaffold, which is loaded with cobalt-doped bioactive glass. The novelty of our system lies in the integration of angiogenic and osteogenic cues within a single injectable scaffold, aiming to enhance both vascularization and bone regeneration simultaneously. We have comprehensively characterized this scaffold in both in vitro and in vivo settings and show that it enhances angiogenesis, osteogenesis, and bone healing.

Materials and methods

Preparation of Bombyx mori silk fibroin solutions

Silk fibroin (SF) solution was prepared using a chemical degumming method, as previously described[7]. Briefly, cocoons of *Bombyx mori* (Iran Silkworm Research Center, Rasht, Iran) were boiled for 30 min (×3) in 0.02 M Na_2CO_3 solution (Merck, Germany) and rinsed with water to remove sericin. After air-drying and dissolution in a ternary solvent of $CaCl_2$:CH_3CH_2OH:H_2O (all from Merck, Germany) with a molar ratio of 1:2:8 at 72 °C for 90 min, the solution was dialyzed. Dialysis was performed with a 10k MWCO membrane in deionized water for 72 h followed by dialysis in 10% w/v polyethylene glycol (10k MW) for 24 h to obtain a concentrated fibroin solution.

Synthesis of bioactive glass

Bioactive glasses (BGs) with different compositions were synthesized using the sol-gel method described in the literature[13]. The synthesis was performed by adding TEOS ($Si(OC_4H_9)_4$) to $_{dd}H_2O$ (1:18 molar ratio) followed by adding nitric acid (HNO_3; for a final 1 molar concentration) as a catalyst. Then, TEP ($(C_2H_5)_3PO_4$), calcium nitrate ($Ca(NO_3)_2.4H_2O$), and sodium nitrate ($NaNO_3$) (all from Merck, Germany) were added individually at 30-minute intervals under continuous magnetic stirring at room temperature. For cobalt-containing BGs, cobalt chloride ($CoCl_2.4H_2O$) (Merck, Germany) was added before adding the calcium precursor. The concentrations of the components were adjusted to make the final nominal compositions of the synthesized BGs as shown in **Table S1**.

The sol was maintained at room temperature for 5 days until it formed a gel. Then, it was transferred to 60°C and left to age for 72 h. Subsequently, the gel was dried by increasing the temperature by 10°C every 24 h until it reached 120°C. It was maintained at 120°C for 5 h and then, the temperature was increased to 650°C with the rate of 3°C.min^{-1}. Afterwards, the gel

was left to cool to room temperature. Finally, the powder was ground and sieved to obtain particles with diameters in the range of 1-10 μm.

Device design and fabrication

A flow-focusing microfluidic device was designed using CAD software (SolidWorks, Dassault Systems) (**Figure S1**) and fabricated using a 3D printing method. In short, the mold was printed using an SLA 3D printer and resin (Anycubic, China), washed with ethanol and isopropyl alcohol, and cured with UV light. Then, a 10:1 mixture of PDMS and its curing agent (Polydimethylsiloxane [SYLGARD™ 184], Dow Corning, MI, USA) were poured into the mold and placed on a 70°C hot plate for 2 h. Finally, the chip was peeled off the mold and bonded on glass with O_2 plasma. The chip was then used to generate microspheres through the water-in-oil (w/o) method[8,14]. For this purpose, the two immiscible fluids including an outer continuous oil phase and an inner aqueous phase, were fed into the chip through Hamilton PTFE tubing (0.023" inside diameter, 0.043" outside diameter) and controlled by a syringe pump (SAMA Instruments, Tehran, Iran).

Synthesis of microspheres and hydrogel scaffolds

To prepare silk fibroin/gelatin (SF/G) aqueous solution, equal volumes of 5% (w/v) SF and 5% gelatin type A (w/v) (Sigma-Aldrich, Germany) were mixed at 60°C. Then, 1.5% w/w of BG particles were dispersed in the SF/G solution by sonication for 7 min. The SF/G solution with or without BG particles was injected at a flow rate of 0.6 mL/h into the inner phase inlet of the chip. At the same time, a mixture of mineral oil and surfactant Span 80 (98:2 v/v) was fed into the outer phase inlet of the chip at a flow rate of 7 mL/h. Using a solution of 0.05% glutaraldehyde in acetone:water (3:1 v/v), the resulting microspheres were cross-linked for 20h at 4°C in the dark. The microspheres were then stirred in a 100 mM aqueous glycine solution

for 2 h to block the residual aldehyde groups of glutaraldehyde followed by rinsing with deionized water.

Microspheres were used for synthesis of hydrogel scaffolds. For this purpose, microspheres were added to a 2% alginate solution (sodium alginate, Sigma-Aldrich, Germany) and mixed for 20 min using a magnetic stirrer. The amount of microsphere was adjusted to achieve a final concentration of 1.5% BG, 5% fibroin, and 5% gelatin (all w/w) in the hydrogel. Afterward, a solution of 1.4% calcium chloride was added as a crosslinker. The hydrogel formed after 30 min and designated as a microsphere-containing hydrogel scaffold (MHS).

Characterization of bioactive glasses and scaffolds

X-ray fluorescence (XRF) spectroscopy: The elemental composition of BGs was determined using a PW2404 spectrometer (Phillips, the Netherlands) with fundamental parameter method. This technique provided precise elemental analysis essential for understanding the material's composition.

Fourier transform infrared (FTIR) spectroscopy: To analyze the chemical structure of scaffold components, spectral data were collected using the Nexus 670 Thermo Nicolet FTIR system (Thermo Electron Corporation, MD, USA). Measurements were taken in the range 450 to 4000 cm^{-1} with a resolution of 1 cm^{-1}, allowing detailed identification of functional groups present in the scaffolds.

X-ray diffraction (XRD): The phase composition of the scaffolds was determined with the Equinox 3000 XRD (Inel, Artenay, France). Data were collected over a 2Θ range of 5° to 80°A with 0.03° steps. This analysis was crucial for identifying crystalline phases within the scaffolds.

Microscope observations: A Zeiss microscope (Carl Zeiss AG, Germany) was used to assess the morphology and size of water-in-oil (w/o) emulsified microspheres. ImageJ software (National Institutes of Health, USA, imagej.net) was employed to quantify microsphere diameters and plot their size distribution as a histogram (n=200 microspheres). Additionally, scanning electron microscopy (SEM) (TESCAN, VEGA3, Czech) was performed on gold-coated microspheres to further examine their surface characteristics.

Mechanical properties: Rheological properties were evaluated using the Dynamic Mechanical Analyzer (Anton Paar, Austria) at room temperature, employing a plate sensor system to assess the shear-thinning behavior of the construct (n=3). For compressive strength testing, the uniaxial mechanical testing machine (ZwickRoell, Germany) was used. Samples with a diameter of 8 mm and a height of 12 mm were prepared. The load was applied until the initial thickness decreased by 70% with the crosshead speed set at 1 mm/min, allowing for the calculation of Young's modulus from the stress-strain curve (n=3).

Inductively coupled plasma optical emission spectroscopy (ICP-OES): Cobalt release from BGs and MHSs was assessed using an Optima 7300V ICP-OES spectrometer (PerkinElmer, MA, USA). Equal amounts of samples (3 mg BGs or MHSs made from 400 µl of microsphere-containing alginate solution) were immersed in 2 ml modified simulated body fluid (SBF) (Partikan Biomaterial Group, Iran). This corresponds to a mass-to-volume ratio of 1.5 mg/ml. The samples were incubated at 37 °C. After various incubation times, supernatants were collected to measure the Co concentration (n=3).

Porosity: The porosity of the scaffold was determined using a common ethanol infiltration method. The samples were freeze-dried, and their dry weights were recorded. The samples were then immersed in absolute ethanol for 15 minutes and the total ethanol volume was

recorded. After removing the scaffolds, the residual ethanol volume was measured, and samples were weighed again (n=3). Porosity was calculated using Equation (1):

$$\text{Porosity}(\%) = \frac{(W_f - W_i)/\rho E\text{thanol}}{V_1 - V_2} \times 100 \quad (1)$$

where W_i: the weight of the dry samples; W_f: the weight of the immersed samples; V_1: the volume of the ethanol with samples; V_2: the remaining volume of ethanol after removing the samples; ρEthanol: density of ethanol.

Swelling: Swelling was assessed by immersing samples in distilled water at room temperature for various time intervals (n=3). The water absorption was calculated using Equation (2):

$$Swelling(\%) = \frac{W_w - W_d}{W_d} \times 100 \quad (2)$$

where W_d: weight of the dry scaffolds; W_w: weight of the wet scaffolds

Biomimetic mineralization: At a mass-to-volume ratio of 1.5 mg/ml scaffolds were immersed in modified simulated body fluid (SBF) (Partikan Biomaterial Group, Iran) at 37°C for 7 days to evaluate biomimetic mineralization (n=3). The formation of mineralized deposits on the scaffold surface was assessed both morphologically and quantitatively after 1 and 7 days of immersion using SEM/EDX (TESCAN, VEGA3, Czech Republic). The Ca/P ratio was calculated using Equation (3):

$$\text{Ca/P ratio} = \frac{(\text{Ca atomic \%})}{(\text{P atomic \%})} \quad (3)$$

The Ca/P ratio greater than 1.67 indicates the formation of hydroxyapatite.

In vitro experiments

Cell culture: Human osteosarcoma cells (Saos-2) and human umbilical vein endothelial cells (HUVECs) were purchased from National Cell Bank, Pasteur Institute, Iran. The HUVEC and Saos-2 were cultured in the F-12k medium containing 100µg/ml heparin and DMEM-F12

medium (both from Gibco, NY, USA), respectively. The media were supplemented with 10% FBS, 100 U/mL penicillin, and 100 μg/mL streptomycin (all from Gibco, NY, USA). The cells were maintained in a humidified incubator at 37°C with 5% CO_2.

Cell viability test: Saos-2 cells viability was assessed using a live-dead assay based on fluorescein diacetate (FDA) and propidium iodide (PI) staining (both from Sigma-Aldrich, Germany). Saos-2 cells were seeded on scaffolds in 48-well culture plates for 7 days. After incubation, cells were washed with PBS, stained with FDA (5 mg/mL) and PI (2 mg/mL), and incubated for 5 min in the dark. The cells were washed with PBS and evaluated using a fluorescent microscope (Optika, Italy). ImageJ software (v.1.52) was used to quantify the live-dead staining images. Cell proliferation was calculated according to the Equation (4):

$$\text{Viable cells } (\%) = \frac{\text{live cells}}{\text{total cell number}} \times 100 \quad (4)$$

where live cells, number of the cells stained green; and total cell number, total number of cells stained both green and red.

Cell distribution and attachment: DAPI staining (Sigma-Aldrich, Germany) was performed to visualize the distribution of cells. Three days after cell seeding on the scaffolds, 300 nM DAPI solution was added to each well, and the samples were incubated for 5 min in the dark. After removing the DAPI solution, the scaffolds were observed under a fluorescence microscope (Optika, Italy).

Scanning electron microscopy: To observe the morphology of the cells on the scaffolds, the cell-seeded scaffolds were fixed with 2.5% glutaraldehyde for 24 h. Then, the samples were dehydrated in solutions with increasing alcohol concentrations (50 to 100%). Afterward, the samples were freeze-dried and analyzed by SEM (TESCAN, VEGA3, Czech Republic).

Formation of mineralized matrix: Alizarin Red S (ARS) staining (ScienCell, CA, USA) was performed to assess the formation of the mineralized matrix. Saos-2 cells were cultured on the scaffolds for 7 days and fixed with 4% formaldehyde for 15 min at room temperature. The samples were incubated in 40 mM ARS and prepared for qualitative and quantitative analysis according to the manufacturer's protocol. Images of each sample were captured by an inverted microscope (Labomed TCM400, CA, USA). For quantitative analysis, after removal of unbound dye by rinsing with $_{dd}H_2O$, the bound dye was solubilized with 10% (v/v) acetic acid according to manufacturer's protocol. The absorbance of the solubilized dye was measured at 405 nm using an ELISA microplate reader (Bio-Rad, CA, USA).

Cell proliferation: Equal numbers of Saos-2 cells were seeded in the culture plates and allowed to adhere for 24 hours, then culture medium was replaced with fresh medium containing equal amounts of scaffolds. MTT assay was performed after 1-7 days of culture with scaffolds. A 0.5 mg/mL solution was prepared from MTT powder (ATOCEL, Austria) in PBS. After the defined culture period, the culture medium was replaced with MTT solution, and the cells were incubated at 37°C for 3 h. After removing the MTT solution, formazan crystals were dissolved in DMSO. The absorbance of the samples was measured at 570 nm with a 630 nm reference using an ELISA microplate reader (Bio-Rad, Hercules, CA, USA). The number of cells for each sample was determined by interpolating the absorbance value on the standard curve. Cell proliferation was calculated according to Equation (5):

$$Cell\ proliferation\ (\%) = \frac{cell\ number_{t}}{cell\ number_{Ctrl}} \times 100 \quad (5)$$

where cell $number_{Ctrl}$: number of cells in the untreated control wells; cell $number_t$: number of cells in the treated wells

Optimum cobalt-doped bioactive glass: according to the results of the above tests, the bioactive glass doped with 5% w/w cobalt was considered to have the optimum concentration of cobalt.

Therefore, in subsequent experiments, the only cobalt-containing scaffold used was alginate hydrogel containing microspheres made from SF/G loaded with bioactive glass doped with 5% w/w cobalt (A-S-G5Co).

Expression of osteogenic and angiogenic genes: Equal numbers of Saos-2 cells or HUVECs were seeded in separate culture plates and allowed to adhere for 24 hours, then culture medium was replaced with fresh medium containing equal amounts of scaffolds. The cells were harvested after 7 and 14 days for real-time RT-PCR analysis. The expressions of osteogenic genes including collagen type I alpha 1 chain (*COL1A1*), RUNX family transcription factor 2 (*RUNX2*), alkaline phosphatase biomineralization associated (*ALPL*) and osteocalcin (*OCN*) were evaluated on the RNA extract of Saos-2 cells. The expressions of angiogenic genes including vascular endothelial growth factor A (*VEGF*) and hypoxia-inducible factor 1 subunit alpha (*HIF1A*) were evaluated on the RNA extract of HUVEC cells. RNeasy Mini Kit (Qiagen, Germany) was used for RNA isolation. Using QuantiTect Reverse Transcription Kit (Qiagen, Germany), cDNA was synthesized from 1 g of RNA following the manufacturer's instructions. The sequences of primers were obtained from OriGene site (www.origene.com) and custom synthesized by SinaClone (Iran) (**Table 1**). Rotor-Gene™ SYBER®Green PCR kit (Qiagen, Germany) and Rotor-Gene Q real-time PCR thermocycler were used for performing the real-time PCR reaction. The amplification process included an initial denaturation step at 94°C for 2 min, followed by 40 cycles of template denaturation at 94°C (15 sec), primer annealing for 20 sec (from 56 to 62°C for each individual primer pair) and primer extension at 72° (25 sec). For each analysis, two independent experiments were performed in triplicates, and gene expression was normalized to the expression level of the housekeeping gene GAPDH[15,16]. Levels of gene expression of Saos-2 cells and HUVECs not exposed to scaffolds were considered as control (Ctrl) and the Pfaffl method was used for quantification of the gene expression levels.

In vivo experiments

This study was approved by the Ethical Committee of the Iran University of Medical Sciences (Approval ID: IR.IUMS.REC.1397.849). All the sample collection and animal study protocols were performed according to the Iranian National Guidelines.

Surgery and implantation: Male Wistar rats weighing 250-300 gr were divided into five groups of six according to the treatments they received including: (1) Ctrl (untreated), (2) ALG (hydrogel not containing microspheres), (3) A-Sphere (alginate hydrogel containing microspheres made from silk fibroin/gelatin [SF/G]), (4) A-S-G (alginate hydrogel containing microspheres made from SF/G loaded with bioactive glass not containing cobalt), and (5) A-S-G5Co (alginate hydrogel containing microspheres made from SF/G loaded with bioactive glass doped with 5% w/w cobalt). The rats were anesthetized by intra-peritoneal injection of xylazine (5 mg/kg) and ketamine (100 mg/kg). Then, an 8-mm defect was created in the calvarium of the rats. Depending on the group of the study, alginate solution with or without microspheres were applied to the calvarial defect using a 23G needle. Then, a solution of 1.4% calcium chloride was applied. After 4 min, the soft tissue covering of the calvarium was sutured (**Figure S2**). The animals were maintained in species-appropriate conditions including 12-hour light/dark cycle, ambient temperature of 22-25°C with 30-60% humidity and ad libitum access to food and water.

Histological observation: At 4 and 12 weeks after surgery, the animals were euthanized by CO_2 inhalation, and both the scaffolds and surrounding skull tissue were harvested. The collected samples were fixed in 4% formaldehyde for 24 h and then decalcified in 14% EDTA for 30 days at room temperature. The decalcified specimens were dehydrated in ascending grades of ethanol (50 to 100%) and embedded in paraffin. After serial sectioning (5μm) of the sample blocks, they were stained with hematoxylin and eosin (H&E) and Masson's trichrome (MT) to assess the development of new bone.

Histomorphometry: To evaluate the formation of regenerated bone, high-resolution images of H&E and MT-stained sections were captured and analyzed by ImageJ software after selecting the edges of the defects. In H&E staining, blood vessels (tubular structures containing red blood cells) and the regenerated tissue area (pink and purple colors) were identified[17]. In Masson's trichrome staining, early new bone tissue (blue color) and mature bone (red color) were identified[17]. In ImageJ, the identified regions of interest (ROI) were selected manually, and their areas were measured. As no blood vessel was formed in the control (Ctrl) group in week 4, all quantifications were made relative to the values measured for the ALG group at fourth week after surgery.

Statistical analysis

Quantitative data were collected and reported as mean ± SD. The Shapiro-Wilk test was used to determine normality of data (all data showed normal distribution). Analysis of variance (ANOVA) followed by Tukey's post-hoc test was performed for comparison of several means and comparison of proportions was performed by $\chi 2$ test. GraphPad Prism 9 (GraphPad Software, Inc., CA, USA) and IBM SPSS Statistics for Windows (Released 2012, Version 21.0, Armonk, NY: IBM Corp) were used for statistical analysis. The statistical significance was defined as $p < 0.05$.

Results

Spectroscopy

X-ray fluorescence (XRF) spectroscopy: The estimated composition of the bioactive glasses (BGs) and the measured elemental compositions are listed in **Table S1**. The molar percentage of the oxides was calculated, assuming all elements are in the oxide form.

Fourier transform infrared (FTIR) spectroscopy: FTIR spectra of the microsphere-containing hydrogel scaffolds (MHSs) loaded with BGs are presented in **Figure 1a**. All four spectra of the scaffolds have similar vibration bands. The silicate peaks at 923 and 1038 cm^{-1} correspond to SiO_{NBO} and v_{asym} (Si-O-Si) within the silicate tetrahedron, respectively. Silicate bands for v_{sym}(Si-O-Si) are also observed at 476 and 744 cm^{-1}. The peaks at 523 and 603 cm^{-1} are attributed to the v_4(P-O-P) bending mode of PO_4^{3-} groups. The bands at 667, 1265 and 1540 cm^{-1} are related to the α form structure of the V, III, and II amides, respectively. The band at 1641 cm^{-1} indicates a random coil structure of amide I in silk fibroin. The observed peak at 1450 cm^{-1} is related to the Schiff base linkage ($R^1CH=NR^2$) formed upon bonding with glutaraldehyde as a crosslinking agent. A small shoulder at 1080 cm^{-1} and the weak band at 2929 cm^{-1} demonstrate (C–C, C–O) stretching and $v_{sym/asym}$ (C-H) in the polysaccharide structure of alginate, respectively.

X-ray diffraction (XRD):

The results of XRD analysis of the scaffolds are depicted in **Figure 1b**. The pattern has a broad range of 14 to 37° (2θ), indicating the presence of an amorphous structure in all samples. Additionally, a distinct peak is observed within the 28 to 34° 2θ range, suggesting a more defined structural feature in this region related to the self-crystallized structure of the glass. Additionally, a broad peak was detected within the 15 to 25° 2θ range, which is a common feature of alginate, gelatin, and fibroin. This peak is attributed to the amorphous nature of these materials.

Microscope observations

Figure 1c shows the light microscope observation of the morphology of water-in-oil (w/o) emulsified microspheres. Also, the size distribution of microspheres is presented. The mean diameter of the microspheres was 278.73±15.56 μm and the diameters of 70% of microspheres were between 260 to 280 μm. A representative SEM image of the microsphere-containing hydrogel scaffolds (MHSs) demonstrates the pores formed between the microspheres that are interconnected within the alginate matrix.

Mechanical Properties

In the rheological test, the continuous flow experiments showed that the viscosity of the microsphere-containing hydrogel scaffold (MHS) decreases with increasing shear rate, suggesting that the MHS is shear-thinning, which is a desirable characteristic for injectable materials (**Figure 1d**).

Compressive stress-strain curves and Young's modulus of microsphere-containing hydrogel scaffolds are presented in Figure **1d**. The data shows that Young's modulus of the hydrogel not containing microspheres is significantly lower than the hydrogels containing microspheres ($p < 0.0001$). It also shows that when microspheres contain BGs, Young's modulus increases significantly ($p < 0.05$). However, as expected, doping of BGs with Co ions, did not affect the Young's modulus ($p > 0.05$).

Inductively coupled plasma optical emission spectroscopy (ICP-OES)

The release of Co ions from BGs and microsphere-containing hydrogel scaffolds (MHSs) is presented in **Figure 2a** and **Table S2**. The ion release analysis demonstrated release of Co ions in all BGs samples. The rate of release increased up to day 6 and decreased thereafter. Each sample showed a distinct pattern of release. The same pattern of release was observed when BGs were incorporated in the hydrogel scaffolds showing that cobalt release is directly related to its concentration in BGs.

Porosity

Porosity data for microsphere-containing hydrogel scaffolds were obtained using the ethanol infiltration method (**Figure 2b**). All samples had high porosity (>80%). The differences of porosities among samples were not statistically significant. As shown in **Figure 1c**, the sizes of the pores were larger than 100μm.

Swelling

All the groups showed strong potential for water absorption up to 48 h (**Figure 2b**). The data suggest that the incorporation of microspheres into the alginate significantly reduced the water uptake capacity (ALG vs all other groups, $p < 0.001$). All the microsphere containing hydrogel scaffolds showed similar water uptake capacities.

Biomimetic mineralization

The deposits formed on the surface of the scaffolds after incubation with modified SBF were assessed by SEM/EDX (**Figure 3**). The EDX spectra revealed that in the alginate hydrogel not containing bioactive glass (ALG and A-Sphere), sodium chloride was the main deposit on the surface and no calcium-rich hydroxyapatite was formed (Ca/P < 1.67). In the hydrogel scaffolds containing BGs the Ca/P ratio of higher than 1.67 indicated formation of calcium-rich hydroxyapatite in the surface of scaffolds[18]. However, the concentration of cobalt ion in the BGs was inversely related to formation of hydroxyapatite, so, that after 24h incubation, no calcium-rich hydroxyapatite was formed when BG was doped with 7% w/w cobalt (A-S-G7Co, Ca/P < 1.67).

Cell viability test

Viability of the Saos-2 cells seeded on the scaffolds was assessed using the FDA/PI live-dead assay where live cells were stained with green fluorescence and dead cells were stained with red fluorescence (**Figure 4a**). Quantification of the live-dead cells (**Figure 4b**) showed that more than 92% of the cells were alive in all groups. It also showed that in the cobalt-containing

scaffolds, viability of the cells is the same as in other scaffolds ($p > 0.05$; non-significant differences).

Cell distribution and adhesion

DAPI staining revealed that the cells adhered to the scaffolds and spread on their surfaces (**Figure 4a**). The cells attached to the scaffolds were identified in the SEM micrographs, which also demonstrated that the scaffolds maintained their structural integrity over the period of cell culture.

Formation of mineralized matrix

ARS staining provided the qualitative and quantitative data presented in **Figure 4 (a, b)**. The data indicates that Saos-2 cells cultured on BG-containing scaffolds showed a significant increase in the formation of mineralized matrix on day 7 compared to the other groups. In the samples containing 5% w/w cobalt-doped bioactive glass (A-S-G5Co) the highest amount of mineralized matrix was formed ($p < 0.0001$). There was no statistically significant difference among the other samples containing BGs ($p > 0.05$).

Cell proliferation

MTT assay was used to evaluate the effect of scaffolds on the proliferation rate of the Saos-2 cells (**Figure 4**). On the first day, there were no statistically significant differences between the groups being compared. On the third day, cell proliferation in the group exposed to the scaffold containing BG doped with 5% w/w cobalt (A-S-G5Co) was higher than the control group ($p<0.05$), while in the group exposed to the scaffold containing BG doped with 7% w/w cobalt (A-S-G7Co), it was lower than all other groups ($p < 0.01$). On day 7, cell proliferation in the A-S-G7Co group was significantly lower than all other groups ($p<0.001$) and the differences among other groups were not significant ($p>0.05$)

Expression of osteogenic and angiogenic genes

The effects of the scaffolds on gene expression in Saos-2 cells and HUVECs are depicted in **Figure 5**. Higher expression of osteogenic genes (*COL1A1*, *ALPL*, *OCN*, and *RUNX2*) was demonstrated in all the SaoS-2 cells exposed to the scaffolds containing BGs as compared with the control and the cells exposed to alginate hydrogel not containing microspheres (ALG). When the BGs were doped with cobalt, expression of *COL1A1*, *ALPL* and *OCN* were significantly increased on day 7 and expression of *OCN* and *RUNX2* were significantly increased on day 14. In HUVECs, exposure to the scaffold containing Co-doped BG significantly enhanced the expression levels of angiogenic genes (*HIF1A* and *VEGF*) in all time points.

In vivo experiments

H&E staining of histological sections: As presented in **Figure 6**, in the untreated group (Ctrl) and the group that received the hydrogel not containing microspheres (ALG), the areas of the regenerated tissues were smaller than the other groups. Also, in the Ctrl group, the defect was only filled with a low-density connective tissue in the fourth week. In week 4, regenerated tissue areas in the groups that received BG-containing hydrogel (A-S-G and A-S-G5Co) were larger than the others. In week 12, new bones were observed connecting the defect margins in both A-S-G and A-S-G5Co groups. Also, the group that received cobalt-doped BG in the hydrogel scaffold (A-S-G5Co) showed more extensive regeneration as compared with the others. No blood vessel was observed in regenerating tissue in the Ctrl group in the fourth week. Blood vessels were detected in the regenerating tissue in all other groups in both time points and in Ctrl group in week 12. Highest density of blood vessels (yellow arrows in **Figure 6**) was observed in A-S-G5Co group showing positive effect of cobalt in angiogenesis.

Masson's trichrome staining of histological sections: **Figure 7** shows early new bone and mature bone in different experimental groups. No new bone formation was observed in the

tissue sections prepared in week 4. In week 12, new bone was identified in the groups that received BG-containing hydrogel scaffolds (A-S-G and A-S-G5Co) and mature bone was only observed in the group that received cobalt-containing scaffold (A-S-G5Co).

Discussion

In this study, injectable microsphere-containing hydrogel scaffolds (MHS) loaded with cobalt-doped bioactive glasses (BGs) were developed and demonstrated to promote bone healing together with angiogenesis in a small mammal (rat) model of bone defects. Microspheres were synthesized using silk fibroin and gelatin (SF/G) in a flow-focusing microfluidic device. Microspheres improve not only the mechanical properties and porosities of an injectable scaffold, but also sustainability of the release of molecules and ions loaded in their structures. Cobalt-doped BG were loaded into the microspheres to take advantage of the osteoconductive and osteoinductive properties of BG and the angiogenic and osteogenic properties of cobalt[19]. Cobalt activates the HIF-1α signaling pathway, promotes a hypoxia-like response, and ultimately enhances angiogenesis in regenerating bone tissue[20]. XRF spectroscopy was used to confirm that the molar percentages of the oxides of the synthesized BGs were consistent with the calculated percentages (slight variations between the nominal and final compositions was ascribed to the impact of the washing process during the sol-gel synthesis)[21].

The FTIR spectra (**Figure 1a**) confirmed the incorporation of BG and biopolymers including alginate, gelatin, and silk fibroin in the scaffolds. The presence of BG in the scaffolds is confirmed by the characteristic silicate and phosphate peaks[22]. The amide bands reflected the proteinaceous nature and secondary structure of gelatin and silk fibroin, which are important for cell adhesion and differentiation. The Schiff base band revealed the crosslinking effect of glutaraldehyde, which enhanced the mechanical and chemical properties of the scaffolds[23]. The FTIR results also imply that the scaffolds had a good interfacial compatibility between the glass and polymer phases, as no significant shifts or changes in the peak positions were observed.

The XRD results (**Figure 1b**) showed that the scaffolds had an amorphous structure with some degree of crystallinity in the glass phase. This is consistent with previous studies that reported

the formation of self-crystallized glass structures in bioactive glass-based scaffolds[22,23]. The amorphous nature of the scaffolds is desirable for bone tissue engineering, as it enhances the bioactivity of the materials[24]. The presence of alginate, gelatin, and fibroin in the scaffolds also contributes to the amorphous structure, as these polymers are known to have low crystallinity and high intake of water.

Visible light microscopy images (**Figure 1c**) showed that the diameters of more than 70% of wet SF/G microspheres were between 260-280 μm after crosslinking, which are within the optimal range for bone tissue engineering[25]. The SEM images showed that the microspheres were well dispersed and adhered to the alginate matrix, forming a porous structure. The pore size of > 100 μm is considered to be the minimum size for bone ingrowth[26]. However, larger pores compromise the mechanical strength, so we aimed to achieve a balance between pore size and strength in our scaffold. The pores are formed due to the well-dispersed nature of the microspheres within the matrix. When the microspheres are mixed into the alginate solution, they occupy specific volumes within the matrix. Upon gelation, these microspheres create interstitial spaces, leading to the formation of pores. The size and distribution of these pores are influenced by the size and concentration of the microspheres.

The rheological properties of our scaffolds showed shear-thinning behavior, which allows them to flow easily through a syringe under applied pressure, and then recover their original viscosity and shape after injection. This can be attributed to the reversible interactions between the alginate and the microspheres. The shear-thinning behavior of the MHS can also reduce the mechanical damage to the cells and tissues during injection. Injectable scaffolds can conform to various defect shapes and sizes without surgical intervention, but bone tissue engineering demands mechanical properties akin to human bone. In the current study, adding BGs to the scaffolds improved their mechanical properties. This finding agrees with previous research,

which showed that alginate composite scaffolds with higher BG contents have enhanced compressive strength and Young's modulus[27]. As it has been reported before, hydrogel scaffolds with compressive strength between ~0.015 to ~1 MPa could effectively replace cancellous bone[28]. Therefore, our BG-containing scaffolds have suitable mechanical properties for filling cancellous bone defects.

We have shown that when microspheres are incorporated into the hydrogel scaffolds (MHSs), the levels of release of cobalt are affected, which is a desirable property in this current study. Cobalt is cytotoxic at high concentrations, yet it can activate the HIF-1α signaling pathway and promote angiogenesis within the biologically relevant range of 3-12 ppm[29]. Our results (**Figure 2a**) indicate that in the MHSs containing cobalt-doped BGs, the release of cobalt from A-S-G5Co group falls within the biological range. Additionally, we observed that the incorporation of microspheres significantly decreased the swelling of the scaffold. This is because the microspheres mechanically interfere with water uptake by the hydrogel, thereby stabilizing its structure and preventing excessive swelling. But, as expected, the composition of the microspheres did not affect the swelling behavior because microspheres mechanically interfere with water uptake by hydrogel scaffolds.

EDX analysis after incubation with modified simulated body fluid (**Figure 3**) showed that calcium rich hydroxyapatite deposits on the surface of BG-containing scaffolds and that the deposition is inversely related with the cobalt content of the BGs. This is in agreement with previous studies reporting that cobalt can lead to formation of cobalt-substituted hydroxyapatite[30] and can interact with phosphate groups and inhibit the nucleation and growth of hydroxyapatite crystals[31].

Our cell culture studies (**Figure 4**) demonstrated that more than 92% of the cells stayed alive when cultured on the surface of the scaffolds, the cells uniformly attach to and spread on the surface and the structural integrity of MHSs is preserved during the period of cells culture. However, we observed a dose-dependent response to cobalt for Saos-2 cells proliferation and deposition of mineralized matrix, consistent with a previous report[32]. Saos-2 cells proliferation and mineralized matrix deposition were significantly reduced by the hydrogel scaffold containing the BG doped with 7% w/w cobalt and matrix deposition was markedly increased by that doped with 5% w/w cobalt.

Based on the results discussed so far, the MHS group containing BG doped with 5% w/w cobalt (A-S-G5Co) was deemed the optimal cobalt-containing hydrogel for this study. Subsequently, only this cobalt-containing scaffold underwent further evaluation for its effects on cellular gene expression and in vivo bone healing. Our results (**Figure 5**) showed that in addition to the expected increase in the expression of osteogenic genes in Saos-2 cells by BG-containing scaffolds, the scaffold containing cobalt-doped BG further increased the expression of *COL1A1*, *ALPL*, and *OCN* on day 7, and *OCN* and *RUNX2* on day 14. On the other hand, the expression of angiogenic genes of *HIF1A* and *VEGF* were markedly increased in HUVECs by the cobalt-containing scaffold in all time points. This confirms that A-S-G5Co scaffold activates both osteogenic and angiogenic signaling pathways, a process known as angiogenesis-osteogenesis coupling[10]. Accordingly, the upregulation of *HIF1A* and *VEGF* in our study is consistent with previous reports defining a key role for these genes in angiogenesis-osteogenesis coupling through activation of a molecular hypoxic cascade[9,10].

The in vivo experiments (**Figures 6** and **7**) confirmed our results that have been discussed above. When the experimental bone defects were treated with MHSs, BG-containing scaffolds promoted the healing process more than others and the cobalt-containing scaffold further

increased the healing after 12 weeks. In the group received cobalt-containing scaffold, the vascularized area measured in the histological study was significantly more than other groups. Also, formation of new bones was observed in the groups received BG-containing scaffolds but, mature bone was only observed in the group received the cobalt-containing scaffold. These show that we have successfully combined the osteogenic- and angiogenic-enhancing properties in the scaffold containing microspheres loaded with 5% w/w cobalt-doped bioactive glasses and promoted bone healing through angiogenesis-osteogenesis coupling.

Conclusion

In this study, we have designed a flow-focusing microfluidic device to synthesize silk fibroin/gelatin microspheres using a water-in-oil emulsification method. The microspheres were loaded with cobalt-doped bioactive glass particles and were incorporated into an alginate hydrogel for bone healing application. The microspheres interacted with each other and created a network of micropores to support cell attachment and proliferation. Also, they improved mechanical strength and mineralized matrix production in vitro. The scaffold containing bioactive glass doped with 5% w/w cobalt released this ion over an extended period, enhanced angiogenic and osteogenic gene expression in vitro, and promoted angiogenesis and bone formation in vivo through the angiogenesis-osteogenesis coupling. However, a few challenges need to be further studied including long-term effects of this scaffold on bone healing and regeneration. Further in vivo studies could also be conducted to evaluate the safety and efficacy of the scaffold in larger animal models and eventually in human clinical trials.

Authors contributions

Parmida Ghiasi Tabari: Conceptualization; Investigation; Methodology; Data curation; Formal analysis; Visualization; Writing -original draft; Writing - review & editing. **Amirmohammad Sattari:** Investigation; Methodology; Data curation; Writing - review & editing. **Mohsen Mashhadi Keshtiban:** Investigation; Methodology; Data curation; Writing - review & editing. **Nushin Karkuki Osguei:** Writing - review & editing. **John G. Hardy:** Methodology; Writing - review & editing. **Ali Samadikuchaksaraei:** Conceptualization; Funding acquisition; Methodology; Project administration; Resources; Software; Supervision; Validation; Visualization; Writing -original draft; Writing - review & editing.

Acknowledgement

The authors would like to thank Iran University of Medical Sciences for its full support of this project. Parts of the graphical abstract were drawn by using pictures from Servier Medical Art by Servier, licensed under a Creative Commons Attribution 3.0 Unported License.

Declaration of competing interest

Ali Samadikuchaksaraei and Ghiasi Tabari are inventors and owners of a patent related to this project, which has been filed in the Iranian Intellectual Property Office but has not been licensed yet. Samadikuchaksaraei is shareholder and CEO of Baztarmim Company, which is focused on production of tissue engineering products. Other authors have no conflicts of interest to declare.

Funding

This study was funded by a grant from Iran University of Medical Sciences (grant number: 97-3-5-12945).

References

1. Kazemi M, Azami M, Johari B, Ahmadzadehzarajabad M, Nazari B, Kargozar S, Hajighasemlou S, Mozafari M, Soleimani M, Samadikuchaksaraei A. Bone Regeneration in rat using a gelatin/bioactive glass nanocomposite scaffold along with endothelial cells (HUVECs). International Journal of Applied Ceramic Technology 2018;15:1427-1438.
2. Rahmati M, Milan PB, Samadikuchaksaraei A, Goodarzi V, Saeb MR, Kargozar S, Kaplan DL, Mozafari M. Ionically crosslinked thermoresponsive chitosan hydrogels formed in situ: A conceptual basis for deeper understanding. Macromolecular Materials and Engineering 2017;302(11):1700227.
3. Zeimaran E, Pourshahrestani S, Fathi A, Razak N, Kadri NA, Sheikhi A, Baino F. Advances in bioactive glass-containing injectable hydrogel biomaterials for tissue regeneration. Acta Biomater 2021;136:1-36.
4. Feng Z, Su X, Wang T, Sun X, Yang H, Guo S. The Role of Microsphere Structures in Bottom-Up Bone Tissue Engineering. Pharmaceutics 2023;15(2):321.
5. Sun M, Gong J, Cui W, Li C, Yu M, Ye H, Cui Z, Chen J, He Y, Liu A. Developments of microfluidics for orthopedic applications: A review. Smart Materials in Medicine 2023;4:111-122.
6. Sinthop S, Patumraj S, Kanokpanont S. Development of gelatin-thai silk fibroin microspheres for three dimensional cell culture. Advanced Materials Research 2014;931:200-204.
7. Johari N, Hosseini HM, Samadikuchaksaraei A. Optimized composition of nanocomposite scaffolds formed from silk fibroin and nano-TiO 2 for bone tissue engineering. Materials Science and Engineering: C, Materials for Biological Applications 2017;79:783-792.
8. Luetchford KA, Chaudhuri JB, Paul A. Silk fibroin/gelatin microcarriers as scaffolds for bone tissue engineering. Materials Science and Engineering: C 2020;106:110116.
9. Diomede F, Marconi GD, Fonticoli L, Pizzicanella J, Merciaro I, Bramanti P, Mazzon E, Trubiani O. Functional Relationship between Osteogenesis and Angiogenesis in Tissue Regeneration. Int J Mol Sci 2020;21(9).
10. Boston B, Ipe D, Capitanescu B, Hamlet S, Love R, Nusem I, Miroiu RI, Warnke PH-H, Petcu EB. Angiogenesis-osteogenesis coupling: a key element in bone physiology and regeneration. 2021(1):2%V 13.
11. Baino F, Montazerian M, Verné E. Cobalt-Doped Bioactive Glasses for Biomedical Applications: A Review. Materials (Basel) 2023;16(14).
12. Deng Z, Lin B, Jiang Z, Huang W, Li J, Zeng X, Wang H, Wang D, Zhang Y. Hypoxia-mimicking cobalt-doped borosilicate bioactive glass scaffolds with enhanced angiogenic and osteogenic capacity for bone regeneration. International journal of biological sciences 2019;15(6):1113.
13. Barrioni BR, de Laia AGS, Valverde TM, da Mata Martins TM, Caliari MV, de Sa MA, de Goes AM, de Magalhães Pereira M. Evaluation of in vitro and in vivo biocompatibility and structure of cobalt-releasing sol-gel bioactive glass. Ceramics International 2018;44(16):20337-20347.
14. Sadeghi D, Solouk A, Samadikuchaksaraei A, Seifalian AM. Preparation of internally-crosslinked alginate microspheres: Optimization of process parameters and study of pH-responsive behaviors. Carbohydrate Polymers 2021;255:117336.
15. Quiroz FG, Posada OM, Gallego-Perez D, Higuita-Castro N, Sarassa C, Hansford DJ, Agudelo-Florez P, López LE. Housekeeping gene stability influences the quantification of osteogenic markers during stem cell differentiation to the osteogenic lineage. Cytotechnology 2010;62(2):109-20.
16. Zhu X, Zhang L, Hu Y, Zhang J. Identification of suitable reference genes for real-time qPCR in homocysteine-treated human umbilical vein endothelial cells. PLoS One 2018;13(12):e0210087.
17. Mohiuddin OA, Campbell B, Poche JN, Ma M, Rogers E, Gaupp D, Harrison MA, Bunnell BA, Hayes DJ, Gimble JM. Decellularized adipose tissue hydrogel promotes bone

regeneration in critical-sized mouse femoral defect model. Frontiers in bioengineering and biotechnology 2019;7:211.
18. Raynaud S, Champion E, Bernache-Assollant D, Thomas P. Calcium phosphate apatites with variable Ca/P atomic ratio I. Synthesis, characterisation and thermal stability of powders. Biomaterials 2002;23(4):1065-72.
19. Liu G, Wang X, Zhou X, Zhang L, Mi J, Shan Z, Huang B, Chen Z, Chen Z. Modulating the cobalt dose range to manipulate multisystem cooperation in bone environment: a strategy to resolve the controversies about cobalt use for orthopedic applications. Theranostics 2020;10(3):1074-1089.
20. Bai H, Wang Y, Zhao Y, Chen X, Xiao Y, Bao C. HIF signaling: A new propellant in bone regeneration. Biomaterials Advances 2022;138:212874.
21. Neščáková Z, Zheng K, Liverani L, Nawaz Q, Galusková D, Kaňková H, Michálek M, Galusek D, Boccaccini AR. Multifunctional zinc ion doped sol–gel derived mesoporous bioactive glass nanoparticles for biomedical applications. Bioactive materials 2019;4:312-321.
22. Jang J-W, Min K-E, Kim C, Shin J, Lee J, Yi S. Scaffold Characteristics, Fabrication Methods, and Biomaterials for the Bone Tissue Engineering. International Journal of Precision Engineering and Manufacturing 2023;24(3):511-529.
23. Manzini BM, Machado LMR, Noritomi PY, da Silva JVL. Advances in Bone tissue engineering: A fundamental review. Journal of Biosciences 2021;46(1):17.
24. Qu H, Fu H, Han Z, Sun Y. Biomaterials for bone tissue engineering scaffolds: a review. RSC Adv 2019;9(45):26252-26262.
25. Chai S, Huang J, Mahmut A, Wang B, Yao Y, Zhang X, Zhuang Z, Xie C, Xu Z, Jiang Q. Injectable Photo-Crosslinked Bioactive BMSCs-BMP2-GelMA Scaffolds for Bone Defect Repair. Front Bioeng Biotechnol 2022;10:875363.
26. Jahir-Hussain MJ, Maaruf NA, Esa NEF, Jusoh N. The effect of pore geometry on the mechanical properties of 3D-printed bone scaffold due to compressive loading. IOP Conference Series: Materials Science and Engineering 2021;1051(1):012016.
27. Zamani D, Moztarzadeh F, Bizari D. Alginate-bioactive glass containing Zn and Mg composite scaffolds for bone tissue engineering. International journal of biological macromolecules 2019;137:1256-1267.
28. Rezwan K, Chen Q, Blaker JJ, Boccaccini AR. Biodegradable and bioactive porous polymer/inorganic composite scaffolds for bone tissue engineering. Biomaterials 2006;27(18):3413-3431.
29. Quinlan E, Partap S, Azevedo MM, Jell G, Stevens MM, O'Brien FJ. Hypoxia-mimicking bioactive glass/collagen glycosaminoglycan composite scaffolds to enhance angiogenesis and bone repair. Biomaterials 2015;52:358-366.
30. Mabilleau G, Filmon R, Petrov P, Baslé M-F, Sabokbar A, Chappard D. Cobalt, chromium and nickel affect hydroxyapatite crystal growth in vitro. Acta biomaterialia 2010;6(4):1555-1560.
31. Nesseri E, Boyatzis SC, Boukos N, Panagiaris G. Optimizing the biomimetic synthesis of hydroxyapatite for the consolidation of bone using diammonium phosphate, simulated body fluid, and gelatin. SN Applied Sciences 2020;2(11):1892.
32. Yang S, Zhang K, Jiang J, James B, Yang SY. Particulate and ion forms of cobalt-chromium challenged preosteoblasts promote osteoclastogenesis and osteolysis in a murine model of prosthesis failure. J Biomed Mater Res A 2019;107(1):187-194.

Graphical abstract

Table 1. The sequences of primers used for real-time RT-PCR assay.

Target gene		
GAPDH	Accession No.	NM_002046.5
	OriGene* catalogue No.	HP205798
	Forward primer sequence (5'→3')	F: GTCTCCTCTGACTTCAACAGCG
	Reverse primer sequence (5'→3')	R: ACCACCCTGTTGCTGTAGCCAA
ALPL	Accession No.	NM_000478.5
	OriGene* catalogue No.	HP200450
	Forward primer sequence (5'→3')	F: GCTGTAAGGACATCGCCTACCA
	Reverse primer sequence (5'→3')	R: CCTGGCTTTCTCGTCACTCTCA
OCN	Accession No.	NM_199173.6
	OriGene* catalogue No.	HP226248
	Forward primer sequence (5'→3')	F: CGCTACCTGTATCAATGGCTGG
	Reverse primer sequence (5'→3')	R: CTCCTGAAAGCCGATGTGGTCA
COL1A1	Accession No.	NM_000088.3
	OriGene* catalogue No.	HP200074
	Forward primer sequence (5'→3')	F: GATTCCCTGGACCTAAAGGTGC
	Reverse primer sequence (5'→3')	R: AGCCTCTCCATCTTTGCCAGCA
RUNX2	Accession No.	NM_004348.3
	OriGene* catalogue No.	HP225916
	Forward primer sequence (5'→3')	F: CCCAGTATGAGAGTAGGTGTCC
	Reverse primer sequence (5'→3')	R: GGGTAAGACTGGTCATAGGACC
VEGF	Accession No.	NM_001025366.3
	OriGene* catalogue No.	HP202779
	Forward primer sequence (5'→3')	F: TTGCCTTGCTGCTCTACCTCCA
	Reverse primer sequence (5'→3')	R: GATGGCAGTAGCTGCGCTGATA
HIF1A	Accession No.	NM_001530.3
	OriGene* catalogue No.	HP205393
	Forward primer sequence (5'→3')	F: TATGAGCCAGAAGAACTTTTAGGC
	Reverse primer sequence (5'→3')	R: CACCTCTTTTGGCAAGCATCCTG

* www.origene.com

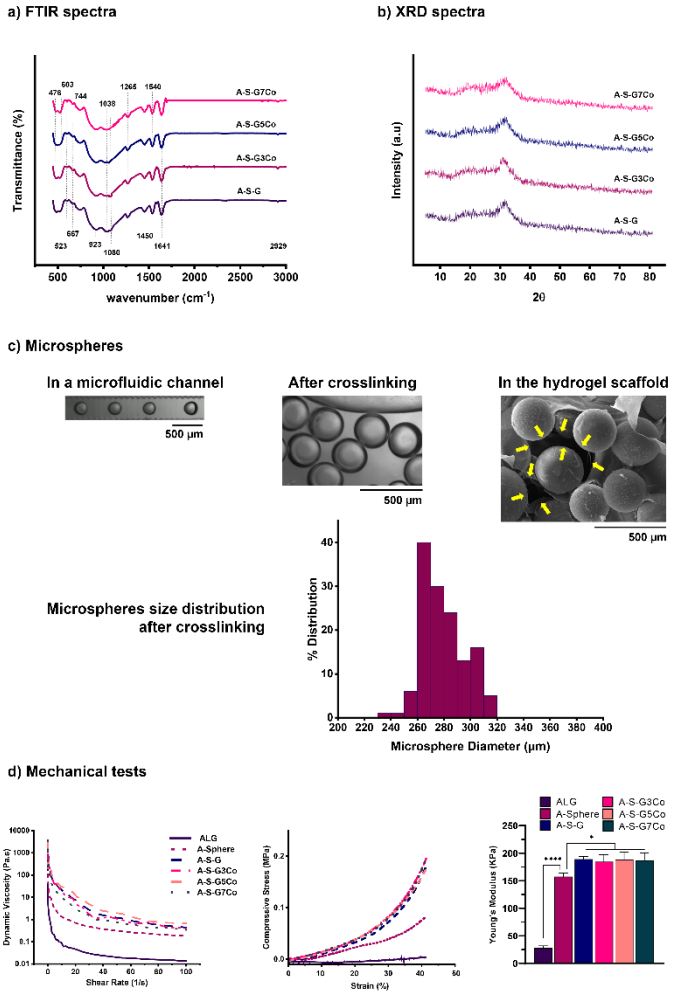

Figure 1. Chemical, structural and mechanical characterization of microspheres and microsphere-containing hydrogel scaffolds (MHSs). Results of (a) FTIR and (b) XRD spectra of scaffolds. (c) Light microscope images of emulsified microspheres inside a channel of the microfluidic device, the final crosslinked microspheres, SEM image of a microsphere-containing hydrogel scaffold showing the micropores with size of >100 µm (yellow arrows) and the mean size distributions of the crosslinked microspheres. (d) Mechanical tests including rheological properties (dynamic viscosity vs. shear rate), compressive stress-strain curve, and Young's modulus of hydrogels in the wet state. (n =3, *p < 0.05; **p < 0.01; ***p < 0.001; ****p <0.0001). ALG: alginate hydrogel not containing microspheres; A-Sphere: alginate hydrogel containing microspheres made from silk fibroin/gelatin (SF/G); A-S-G: alginate hydrogel containing microspheres made from SF/G loaded with bioactive glass not containing cobalt; A-S-GxCo: alginate hydrogel containing microspheres made from SF/G loaded with bioactive glass doped with 3%, 5% and 7% w/w cobalt.

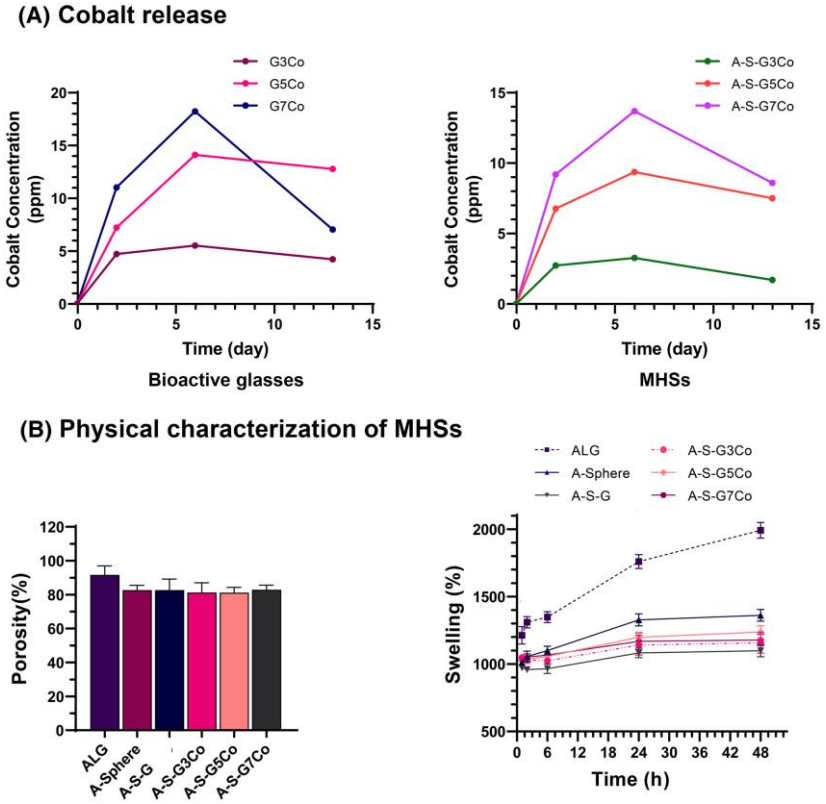

Figure 2. Multifaceted Characterization of bioactive glasses and microsphere-containing hydrogel scaffolds (MHSs). (a) Cobalt release from bioactive glasses and (b) physical characterization of MHSs including measurement of porosity (in absolute ethanol) and swelling (in distilled water). MHSs: microsphere-containing hydrogel scaffolds; ALG: alginate hydrogel not containing microspheres; A-Sphere: alginate hydrogel containing microspheres made from silk fibroin/gelatin (SF/G); A-S-G: alginate hydrogel containing microspheres made from SF/G loaded with bioactive glass not containing cobalt; A-S-GxCo: alginate hydrogel containing microspheres made from SF/G loaded with bioactive glass doped with 3%, 5% and 7% w/w cobalt.

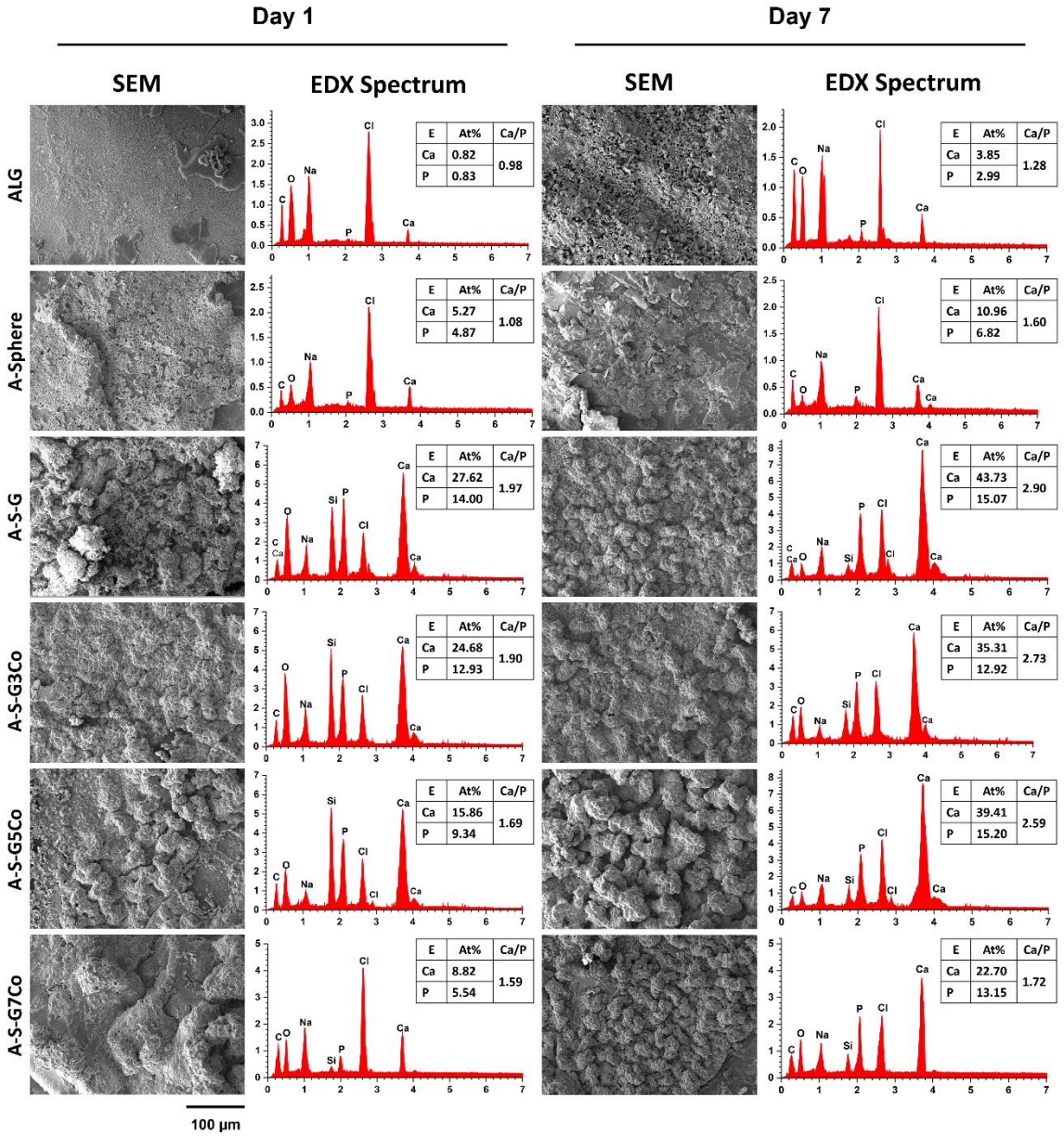

Figure 3. SEM/EDX analysis. The images enable analysis of the biomimetic mineralization of the scaffolds after incubation in modified simulated body fluid for 1 and 7 days; SEM images shows the deposition formation on the surface of scaffolds; EDX spectra reveals the proportion of elements in the deposits (scale bar 100 µm for all SEM images). ALG: alginate hydrogel not containing microspheres; A-Sphere: alginate hydrogel containing microspheres made from silk fibroin/gelatin (SF/G); A-S-G: alginate hydrogel containing microspheres made from SF/G loaded with bioactive glass not containing cobalt; A-S-GxCo: alginate hydrogel containing microspheres made from SF/G loaded with bioactive glass doped with 3%, 5% and 7% w/w cobalt; E: elements; At%: atom%.

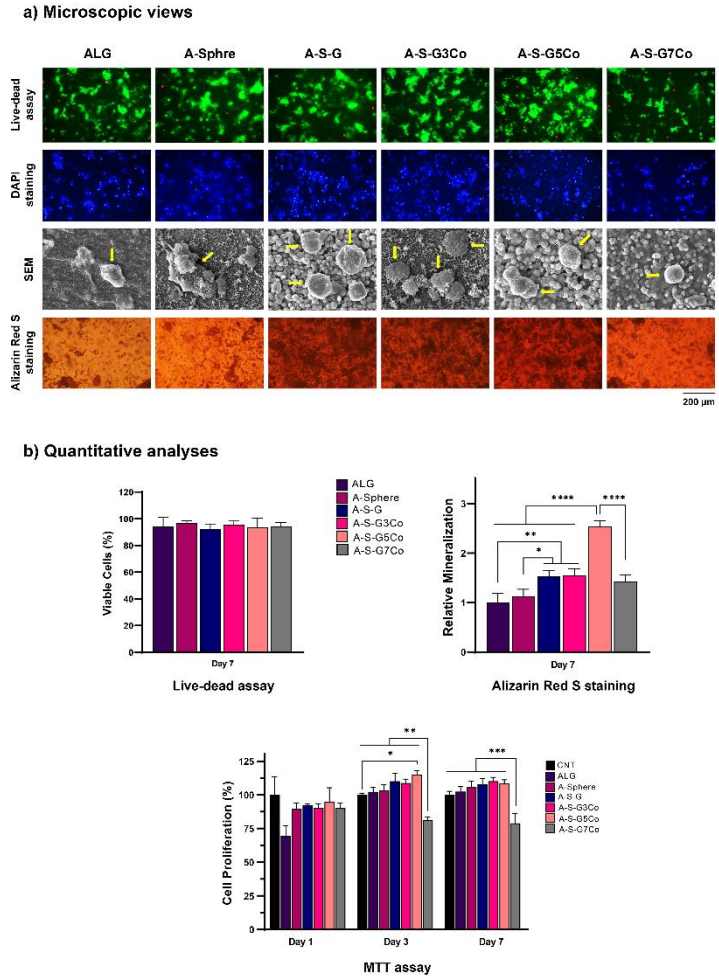

Figure 4. Cellular experiments. (a) Optical microscopic view of the live-dead assay at day 7 showing the live cells stained green and dead cells stained red; DAPI staining showing the distribution of osteoblasts on the scaffolds at day 3; SEM images of the cells attached to scaffolds at day 3 (yellow arrows); and Alizarin Red S (AS) staining for visualization of biomimetic mineralization at day 7; (b) quantitative analysis of live-dead assay; quantitative analysis of ARS staining; and the effects of scaffolds on cellular proliferation. Data are presented as the mean ± SD. (n =3, *p < 0.05; **p < 0.01; ***p < 0.001; ****p <0.0001; scale bar 200 µm for all microscopic images). CNT: Control (cells not exposed to scaffolds); ALG: alginate hydrogel not containing microspheres; A-Sphere: alginate hydrogel containing microspheres made from silk fibroin/gelatin (SF/G); A-S-G: alginate hydrogel containing microspheres made from SF/G loaded with bioactive glass not containing cobalt; A-S-GxCo: alginate hydrogel containing microspheres made from SF/G loaded with bioactive glass doped with 3%, 5% and 7% w/w cobalt.

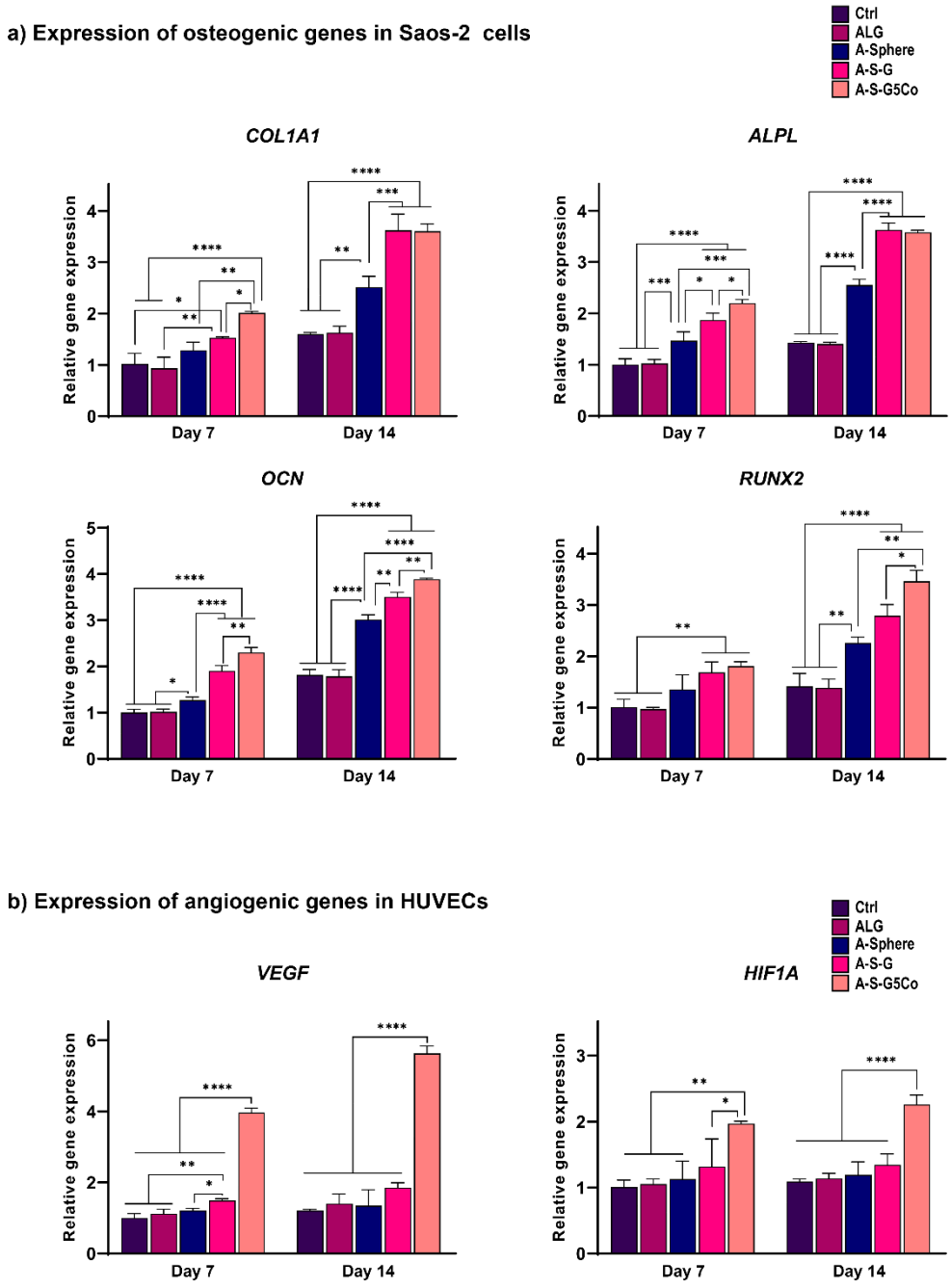

Figure 5. Gene expression study. Expression levels of (a) osteogenic genes in Saos2 cells and (b) angiogenic genes in HUVECs cultured with hydrogel scaffolds for 7 and 14 days. Data are presented as the mean ± SD. (n =3, *p < 0.05; **p < 0.01; ***p < 0.001 and ****p <0.0001). Ctrl: Control (cells not exposed to scaffolds); ALG: alginate hydrogel not containing microspheres; A-Sphere: alginate hydrogel containing microspheres made from silk fibroin/gelatin (SF/G); A-S-G: alginate hydrogel containing microspheres made from SF/G loaded with bioactive glass not containing cobalt; A-S-G5Co: alginate hydrogel containing microspheres made from SF/G loaded with bioactive glass doped with 5%w/w cobalt.

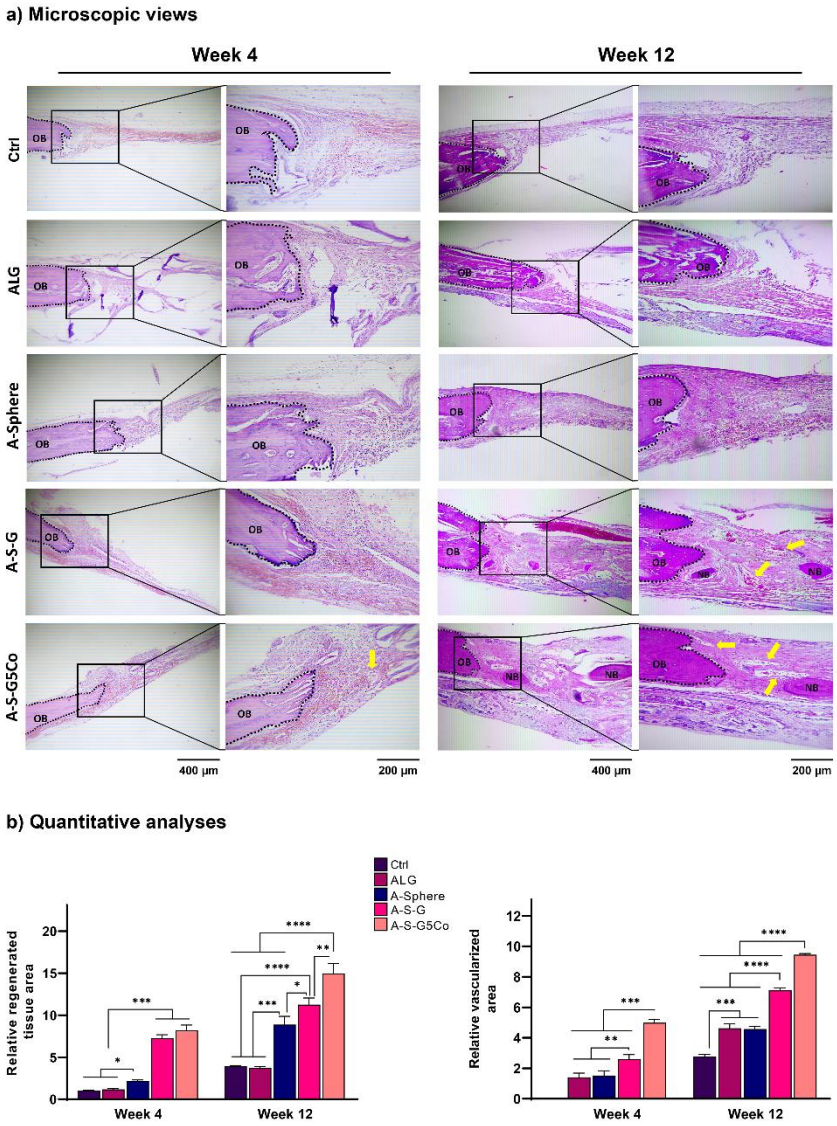

Figure 6. Hematoxylin and Eosin staining. (a) Optical microscope images of H&E stained regenerating tisue; the margins of the untouched bone surrounding the defect (OB, old bone) on the left are marked by dotted lines separaing it from the newly formed tissue. Neovascularizations are marked by yellow arrows; the insets in the first and third columns are shown by a higher magnification in the second and fourth columns; the scale bars for each column (400 µm and 200 µm) are shown at the bottom; (b) Relative comparison of experimental groups for regenerating and vascularized areas in newly formed tissues (n=3, *p < 0.05; **p < 0.01; *** p < 0.001). OB: old bone; NB: new bone; Ctrl: Control (untreated); ALG: alginate hydrogel not containing microspheres; A-Sphere: alginate hydrogel containing microspheres made from silk fibroin/gelatin (SF/G); A-S-G: alginate hydrogel containing microspheres made from SF/G loaded with bioactive glass not containing cobalt; A-S-G5Co: alginate hydrogel containing microspheres made from SF/G loaded with bioactive glass doped with 5%w/w cobalt.

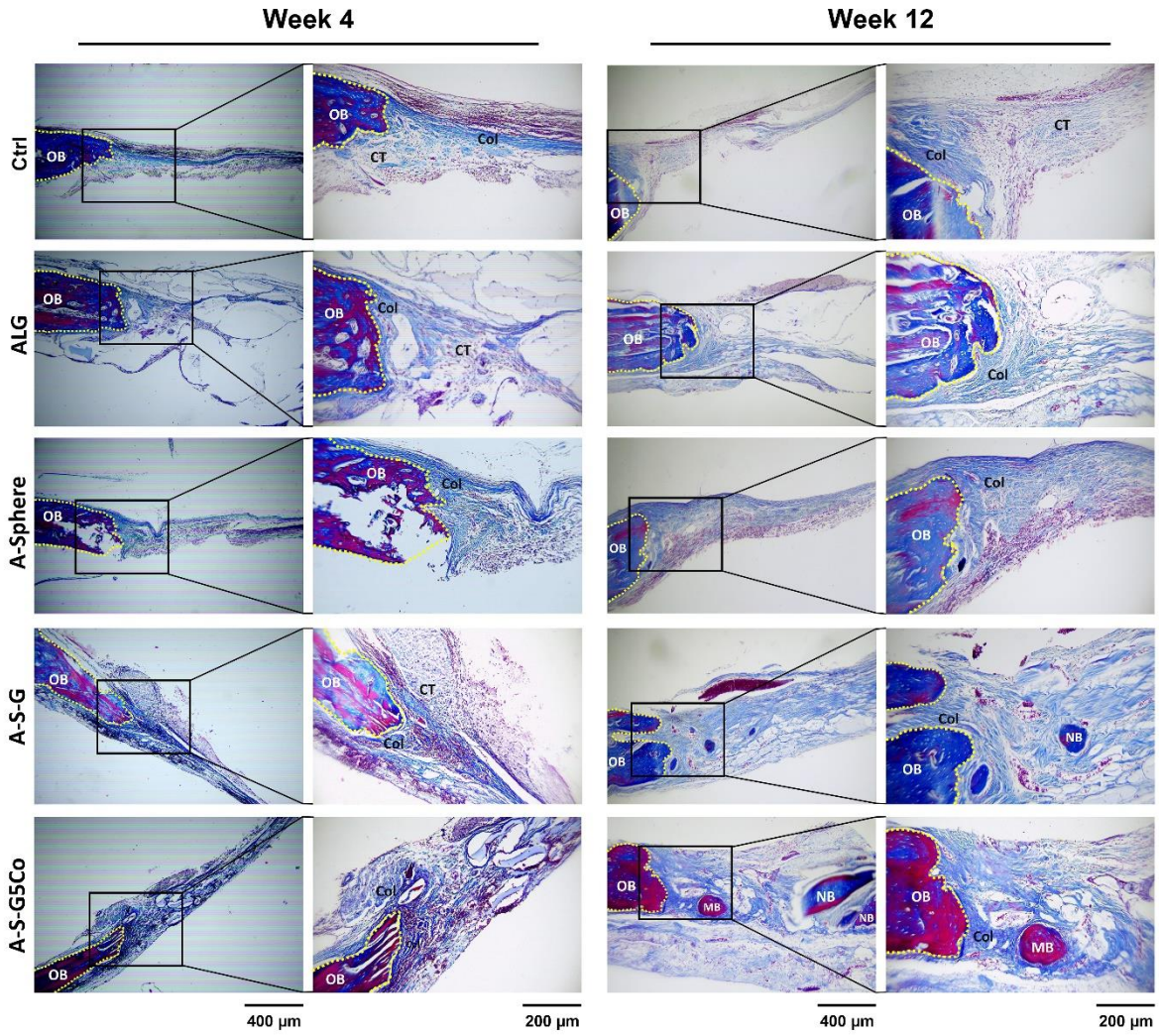

Figure 7. Masson's trichrome staining. Optical microscope images of regenerating tissue; the margins of the untouched bone surrounding the defect (OB, old bone) on the left are marked by dotted lines separaing it from the newly formed tissue; the insets in first and third columns are shown by a higher magnification in the second and fourth columns; the scale bars for each column (400 µm and 200 µm) are shown at the bottom. OB: old bone; NB: new bone; MB: mature bone; Col: collagen content; CT: connective tissue; Ctrl: Control (untreated); ALG: alginate hydrogel not containing microspheres; A-Sphere: alginate hydrogel containing microspheres made from silk fibroin/gelatin (SF/G); A-S-G: alginate hydrogel containing microspheres made from SF/G loaded with bioactive glass not containing cobalt; A-S-G5Co: alginate hydrogel containing microspheres made from SF/G loaded with bioactive glass doped with 5%w/w cobalt.